Geomechanics and Engineering, *Vol. 20, No. 1 (2020) 43-54*
DOI: https://doi.org/10.12989/gae.2020.20.1.043

Reliability analysis of anti-seismic stability of 3D pressurized tunnel faces by response surfaces method

Biao Zhang*[1,3,4], Zongyu Ma[2], Xuan Wang[4], Jiasheng Zhang[4] and Wenqing Peng[2]

[1]*School of Civil Engineering, Hunan University of Science and Technology, Hunan 411201, China*
[2]*School of Resource and Environment and Safety Engineering, Hunan University of Science and Technology, Hunan, 411201, China*
[3]*Hunan Province Key Laboratory of Geotechnical Engineering Stability Control and Health Monitoring, Hunan University of Science and Technology, Hunan 411201, China*
[4]*School of Civil Engineering, Central South University, Hunan 410075, China*

(Received October 11, 2019, Revised December 20, 2019, Accepted December 26, 2019)

Abstract. The limit analysis and response surfaces method were combined to investigate the reliability of pressurized tunnel faces subjected to seismic force. The quasi-static method was utilized to introduce seismic force into the tunnel face. A 3D horn failure mechanism of pressurized tunnel faces subjected to seismic force was constructed. The collapse pressure of pressurized tunnel faces was solved by the kinematical approach. The limit state equation of pressurized tunnel faces was obtained according to the collapse pressure and support pressure. And then a reliability model of pressurized tunnel faces was established. The feasibility and superiority of the response surfaces method was verified by comparing with the Monte Carlo method. The influence of the mean of soil parameters and support pressure, variation coefficients, distribution type and correlation of c-φ on the reliability of pressurized tunnel faces was discussed. The reasonable safety factor and support pressure required by pressurized tunnel faces to satisfy 3 safety levels were presented. In addition, the effects of horizontal seismic force, vertical seismic force and correlation of k_h-k_v on the reliability of pressurized tunnel faces were also performed. The method of this work can give a new idea for anti-seismic design of pressurized tunnel faces.

Keywords: 3D failure mechanism; pseudo-static method; response surfaces method; reliability; correlation

1. Introduction

Shield construction method has been widely popularized and applied in subway because of its advantages of fast and high efficiency. However, the instability of tunnel faces has occurred frequently in the construction process of pressurized tunnel. It not only seriously affects the construction progress, but also may lead to collapse of tunnel faces, and huge casualties and economic losses will be caused.

To prevent the soils instability before tunnel faces, the method of controlling support pressure is usually adopted in engineering. Therefore, determining the support pressure needed to preserve the stability of tunnel faces is a key problem, and it needs to be solved urgently at this stage (Sahoo and Kumar 2019, Shrestha and Panthi 2014, Senent *et al*. 2013, Anagnostou and Perazzelli 2013, Kim and Tonon 2010, Huang *et al*. 2020, Wu *et al*. 2019). Leca and Dormieux (1990) constructed a 2D failure mode of pressurized tunnel faces, and solved the support pressure required by faces with kinematical approach. Yang *et al*. (2015) constructed a 2D multi-block failure mode of tunnel faces. The support pressure and potential damage surfaces under different saturation were obtained with upper bound method. Liang *et al*. (2016) established a 2D failure mode of tunnel faces with logarithmic helical curve. The influence of soil heterogeneity on support pressure of faces was studied with kinematical approach. Zhang *et al*. (2019a) considering the stability of pressurized tunnel faces in unsaturated soil, the analytical solution of support pressure was derived by kinematical approach.

All of the above studies simplify the problem of determining the support pressure of pressurized tunnel faces to a 2D plane strain problem. In fact it belongs to a 3D problem. So some scholars solve the support pressure of pressurized tunnel faces with 3D models. Subrin and Wong (2002) presented a 3D failure mode of the pressurized tunnel faces by using logarithmic helical curve. The expression of support pressure is deduced by the kinematical approach. Saada *et al*. (2013) solved the support pressure of pressurized tunnel faces subjected to seismic effect based on 3D failure mode. Zhang *et al*. (2018) used the upper bound theorem and non-linear failure criterion to solve support pressure of 3D pressurized tunnel faces. Compared with engineering measurements, the correctness is verified. In addition, some scholars used the "point-to-point" method to construct the 3D failure mode of pressurized tunnel faces. The kinematical approach was used to ascertain support pressure needed for faces (Mollon *et al*. 2011, Ibrahim *et al*. 2015, Pan and Dias 2018, Hernández *et al*. 2019).

To sum up, in recent years, scholars over the world have done a lot of work on determining the support pressure of pressurized tunnel faces with kinematical approach. These

*Corresponding author, Ph.D.
E-mail: 1020176@hnust.edu.cn

http://www.techno-press.org/?journal=gae&subpage=7
ISSN: 2005-307X (Print), 2092-6219 (Online)

studies are mainly embodied in the continuous improvement of the failure mode, from the flattening to the rotation, from 2D to 3D. The support pressure of faces is also more accurate. However, the kinematical approach is a fixed value method, which can't consider the discrete nature of soil parameters and objectively existing loads. Also it can't quantitatively analyze the failure probability of tunnel surfaces. Therefore, in this paper, the kinematical approach and response surfaces method are combined to solve the reasonable safety coefficient, support pressure and corresponding failure probability needed to preserve the stability of the tunnel faces. It can provide theoretical basis for pressurized tunnel support design.

2. Methods

2.1 Quasi-static method

The quasi-static method is a simple method to solve the dynamic problem. In essence, the dynamic effect of earthquake is simplified to a constant acceleration in horizontal and vertical directions. The horizontal and vertical acceleration coefficients are expressed with k_h and k_v respectively. The expression is (Clot *et al*. 2016, Zhang *et al*. 2017):

$$k_{\mathrm{v}} = \zeta k_{\mathrm{h}} \tag{1}$$

in which the proportional coefficient ζ is generally valued -1.0, -0.5, 0, 0.5, 1.0. Due to the relationship between the acceleration coefficient k_h and k_v, there is a correlation between the horizontal and vertical seismic force, which is positive correlation or negative correlation. The range of correlation coefficient $\rho_{k_{\mathrm{h}},k_{\mathrm{v}}}$ is -1.0~1.0.

2.2 Upper bound method of limit analysis

For the velocity field of arbitrary maneuvering allowable, the upper bound solution of the failure load can be obtained according to the internal energy loss rate is not less than the external force power. The expression is (Huang *et al*. 2017, Zhang *et al*. 2019b):

$$\int_V \sigma_{ij}\dot{\varepsilon}_{ij}\mathrm{d}V \geq \int_s T_i v_i \mathrm{d}s + \int_V F_i v_i \mathrm{d}V \tag{2}$$

where T_i is the surfaces force acting on the surfaces area s of damage body, F_i is the physical force on the volume V of damage area, σ_{ij} represents the stress field associated with F_i and T_i, v_i is the maneuvering allowable velocity field, $\dot{\varepsilon}_{ij}$ represents the strain rate field compatible with v_i.

2.3 Response surfaces method

The response surfaces method can effectively analyze the reliability of engineering. It has high calculation accuracy and efficiency. To a certain extent, it can meet the needs of engineering design. The calculation idea is to select an explicit function to replace the complex implicit one, and then use the matrix method to solve the reliability of engineering project (Su *et al*. 2007, Zhang *et al*. 2020, Zhang *et al*. 2019c).

3. Calculation model

3.1 A 3D horn failure mode under seismic effect

When a pressurized tunnel is excavated, the disturbance to the soils will be caused. If the support pressure is not enough, it can collapse easily. A large number of works show that the collapse shape of tunnel faces is very similar to the logarithmic spiral curve (Subrin and Wong 2002, Mollon *et al*. 2011). So the logarithmic helical curve is used to construct a 3D collapse mode of tunnel faces subjected to seismic effect, which is also called the horn damage mode.

As shown in Fig. 1, in the excavation process of pressurized tunnel, the faces collapsed under the action of horizontal and vertical seismic force k_hG and k_vG. The horn damage area *AEB* rotates failure around *O* point at angular velocity *w*. Moreover, the intersection area of the horn damage area *AEB* and the circle of tunnel faces *AMBN* is *AM'BN'*. To simplify the calculation, existing literature (Subrin and Wong 2002) assumed that the area formed by intersecting is the *AMBN* circle. In fact, only when the rotation point *O* is directly above point *A*, the area formed by the intersection is the tunnel faces circle *AMBN*, otherwise the area is the pear shape *AM'BN'*. In addition, pressurized tunnel faces diameter is *D*, buried deep is *C*. The damage area *AEB* is composed of logarithmic helical curves. Among them, on the logarithmic spiral curve *AE* and *BE*, the radius vector *OA* and *OB* of point *A* and point *B* are r_a and r_b respectively. The angles of *OB*, *OA*, *OE* and vertical lines are θ_1, θ_2 and θ_3 respectively. A straight line crossing point *O* intersects with *AE* and *BE* at A_i and B_i, respectively. The length of the radius vector OA_i and OB_i is r_1 and r_2, respectively. The plane where A_i and B_i are located is the tangential circle of the horn.

As shown in circles 1-1 and 2-2, the distance from the circle center to *O* Point is r_m, the radius is *R*. The coordinate system is set up with the center of the circle, the direction of OB_i is the direction of *Y* axis. The angle between any point on the arc and the direction of *Y* axis is α, the ordinate is *y*, the angle between the end of the arc and the direction of *y* axis is α_0, and the ordinate is *l*.

According to the geometric relationship in Fig. 1:

$$r_1(\theta) = r_{\mathrm{a}} \exp[(\theta - \theta_2)\tan\varphi] \tag{3}$$

$$r_2(\theta) = r_{\mathrm{b}} \exp[(\theta_1 - \theta)\tan\varphi] \tag{4}$$

$$r_{\mathrm{a}} = \frac{\sin\theta_1}{\sin(\theta_2 - \theta_1)} D \tag{5}$$

$$r_{\mathrm{b}} = \frac{\sin\theta_2}{\sin(\theta_2 - \theta_1)} D \tag{6}$$

$$\theta_3 = \frac{1}{2}[(\theta_1 + \theta_2) - \frac{\ln(\sin\theta_1 / \sin\theta_2)}{\tan\varphi}] \tag{7}$$

$$r_{\mathrm{m}} = (r_1 + r_2)/2 \tag{8}$$

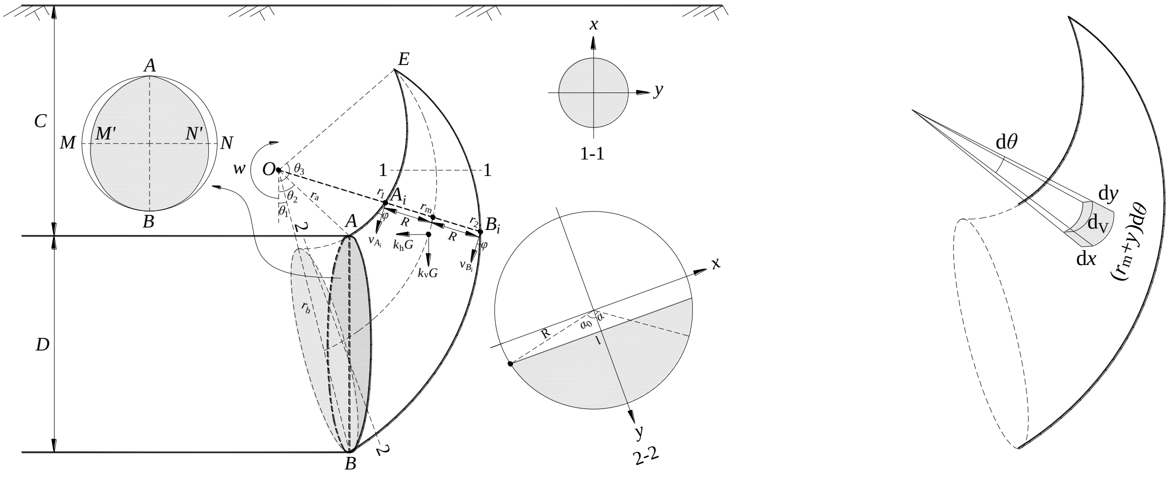

(a) (b)

Fig. 1 3D model of pressurized tunnel faces under seismic effect: (a) The horn failure mode and (b) Volume of microelement

$$R = (r_2 - r_1)/2 \tag{9}$$

$$\cos\alpha_0 = l/R \tag{10}$$

$$r_{\mathrm{m}} + l = r_{\mathrm{a}} \cdot \sin\theta_2/\sin\theta \tag{11}$$

$$v = w \cdot (r_{\mathrm{m}} + y) \tag{12}$$

$$\mathrm{d}V = (r_{\mathrm{m}} + y) \cdot \mathrm{d}x \cdot \mathrm{d}y \cdot \mathrm{d}\theta \tag{13}$$

3.2 Upper bound solution

3.2.1 Basic assumptions

In this paper, the following assumptions are made in the calculation: (1) The effect of seismic effect on shear strength of soil is not considered; (2) The collapse pressure σ_c evenly distributed on tunnel faces. In the limit failure state (safety factor F_s=1), the required support pressure of tunnel faces to maintain stability is equal to the collapse pressure, $\sigma_{\mathrm{T}}=\sigma_c$.

3.2.2 Collapse pressure

From Fig. 1, it can be seen that the horn failure area *AEB* slides under external forces, and energy dissipation occurs during the sliding process of the horn failure area *AEB*. According to the kinematical approach, the power done by external forces includes the power generated by the soil weight $\dot{W}_1$ in horn area, the power generated by the seismic force $\dot{W}_2$, and the power generated by the support pressure $\dot{W}_3$. The internal dissipation rate of $\dot{W}_4$ occurs on the velocity discontinuity of the horn *AEB*.

The power generated by the soil weight is:

$$\begin{aligned}\dot{W}_1 = &\int_{\theta_2}^{\theta_3}\int_{-R}^{R}\int_0^{\sqrt{R^2-y^2}} 2\cdot w\cdot\gamma\cdot(r_{\mathrm{m}}+y)^2\cdot\sin\theta\mathrm{d}x\mathrm{d}y\mathrm{d}\theta \\ &+\int_{\theta_1}^{\theta_2}\int_{l}^{R}\int_0^{\sqrt{R^2-y^2}} 2\cdot w\cdot\gamma\cdot(r_{\mathrm{m}}+y)^2\cdot\sin\theta\mathrm{d}x\mathrm{d}y\mathrm{d}\theta\end{aligned} \tag{14}$$

The total power of seismic forces in both horizontal and vertical directions is:

$$\begin{aligned}\dot{W}_2 = &k_{\mathrm{v}}\cdot\int_{\theta_2}^{\theta_3}\mathrm{d}\theta\int_{-R}^{R}\mathrm{d}y\int_0^{\sqrt{R^2-y^2}} 2\cdot w\cdot\gamma\cdot(r_{\mathrm{m}}+y)^2\cdot\sin\theta\mathrm{d}x + \\ &k_{\mathrm{v}}\cdot\int_{\theta_1}^{\theta_2}\mathrm{d}\theta\int_{l}^{R}\mathrm{d}y\int_0^{\sqrt{R^2-y^2}} 2\cdot w\cdot\gamma\cdot(r_{\mathrm{m}}+y)^2\cdot\sin\theta\mathrm{d}x + \\ &k_{\mathrm{h}}\cdot\int_{\theta_2}^{\theta_3}\mathrm{d}\theta\int_{-R}^{R}\mathrm{d}y\int_0^{\sqrt{R^2-y^2}} 2\cdot w\cdot\gamma\cdot(r_{\mathrm{m}}+y)^2\cdot\cos\theta\mathrm{d}x + \\ &k_{\mathrm{h}}\cdot\int_{\theta_1}^{\theta_2}\mathrm{d}\theta\int_{l}^{R}\mathrm{d}y\int_0^{\sqrt{R^2-y^2}} 2\cdot w\cdot\gamma\cdot(r_{\mathrm{m}}+y)^2\cdot\cos\theta\mathrm{d}x\end{aligned} \tag{15}$$

The power generated by the support pressure is:

$$\dot{W}_3 = \sigma_{\mathrm{T}}\cdot\int_{\theta_1}^{\theta_2}\int_0^{\sqrt{R^2-l^2}} 2\cdot w\cdot(r_{\mathrm{m}}+l)^2\cdot\cos\theta/\sin\theta\,\mathrm{d}x\mathrm{d}\theta \tag{16}$$

The internal dissipation rate is:

$$\begin{aligned}\dot{W}_4 = &\int_{\theta_2}^{\theta_3}\int_0^{\pi} 2\cdot w\cdot c\cdot R\cdot(r_{\mathrm{m}}+R\cdot\cos\alpha)^2\,\mathrm{d}\alpha\mathrm{d}\theta \\ &+\int_{\theta_1}^{\theta_2}\int_0^{\alpha_0} 2\cdot w\cdot c\cdot R\cdot(r_{\mathrm{m}}+R\cdot\cos\alpha)^2\,\mathrm{d}\alpha\mathrm{d}\theta\end{aligned} \tag{17}$$

According to the power equation constructed by external force equal to internal dissipation rate, the collapse pressure of pressurized tunnel faces under seismic effect can be deduced based on this equation:

$$\begin{aligned}&\sigma_{\mathrm{c}} = \sigma_{\mathrm{T}} \\ &= \frac{\dot{W}_1+\dot{W}_2-\dot{W}_4}{\int_{\theta_1}^{\theta_2}\int_0^{\sqrt{R^2-l^2}} 2\cdot w\cdot(r_{\mathrm{m}}+l)^2\cdot\cos\theta/\sin\theta\,\mathrm{d}x\mathrm{d}\theta}\end{aligned} \tag{18}$$

The constraint conditions for the formula are:

$$\text{Subjected to }\begin{cases}0<\theta_1<\theta_2<\pi/2 \\ \theta_2<\theta_3<\pi \\ r_{\mathrm{a}}<r_{\mathrm{b}}\end{cases} \tag{19}$$

3.2.3 Reliability

To ensure the safety, the safety factor must be considered in the support design. According to the collapse pressure σ_c of previous solution, the safety factor F_s is

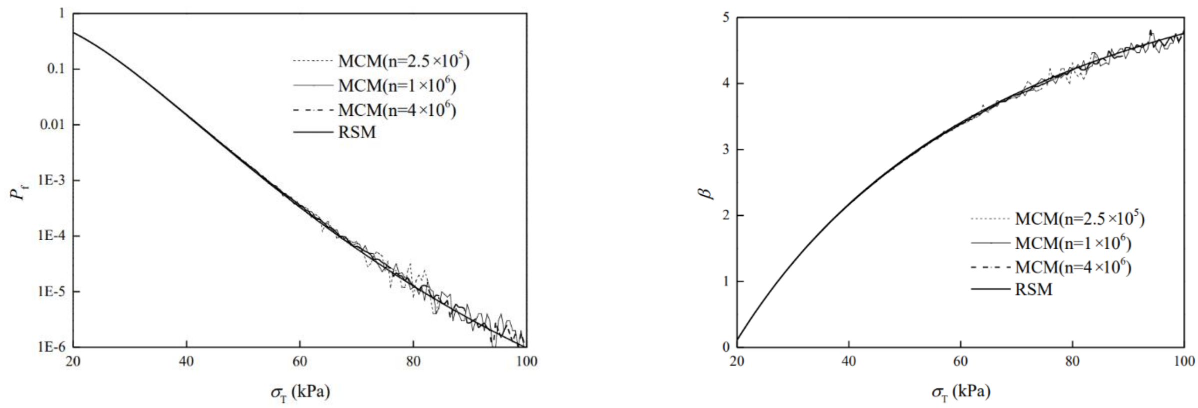

(a) (b)

Fig. 2 Comparisons between Monte Carlo method and response surfaces method: (a) Failure probability and (b) Reliability index

introduced. The support pressure acting on tunnel faces during the excavation of the pressurized tunnel is as follows:

$$\begin{aligned}\sigma_{\mathrm{T}} &= F_{\mathrm{s}} \cdot \sigma_{\mathrm{c}} \\ &= F_{\mathrm{s}} \cdot \frac{\dot{W}_1 + \dot{W}_2 - \dot{W}_4}{\int_{\theta_1}^{\theta_2}\int_0^{\sqrt{R^2-l^2}} 2 \cdot w \cdot \left(r_{\mathrm{m}}+l\right)^2 \cdot \cos\theta \big/ \sin\theta \,\mathrm{d}x\mathrm{d}\theta}\end{aligned} \tag{20}$$

The limit state equation of tunnel faces is constructed according to the support pressure and the collapse pressure:

$$\begin{aligned} g(X) &= \sigma_{\mathrm{T}} - \sigma_{\mathrm{c}} \\ &= (F_{\mathrm{s}}-1) \cdot \frac{\dot{W}_1 + \dot{W}_2 - \dot{W}_4}{\int_{\theta_1}^{\theta_2}\int_0^{\sqrt{R^2-l^2}} 2 \cdot w \cdot \left(r_{\mathrm{m}}+l\right)^2 \cdot \cos\theta \big/ \sin\theta \,\mathrm{d}x\mathrm{d}\theta} \\ &= 0 \end{aligned} \tag{21}$$

According to Eq. (21), the reliability model of pressurized tunnel faces subjected to seismic force is as follows:

$$\begin{aligned} R_{\mathrm{s}} &= P\{g(X) = \sigma_{\mathrm{T}} - \sigma_{\mathrm{c}} > 0\} \\ &= P\left\{(F_{\mathrm{s}}-1) \cdot \frac{\dot{W}_1 + \dot{W}_2 - \dot{W}_4}{\int_{\theta_1}^{\theta_2}\int_0^{\sqrt{R^2-l^2}} 2 \cdot w \cdot \left(r_{\mathrm{m}}+l\right)^2 \cdot \cos\theta \big/ \sin\theta \,\mathrm{d}x\mathrm{d}\theta} > 0\right\} \end{aligned} \tag{22}$$

$$\begin{aligned} P_{\mathrm{f}} &= 1 - R_{\mathrm{s}} \\ &= 1 - P\left\{(F_{\mathrm{s}}-1) \cdot \frac{\dot{W}_1 + \dot{W}_2 - \dot{W}_4}{\int_{\theta_1}^{\theta_2}\int_0^{\sqrt{R^2-l^2}} 2 \cdot w \cdot \left(r_{\mathrm{m}}+l\right)^2 \cdot \cos\theta \big/ \sin\theta \,\mathrm{d}x\mathrm{d}\theta} > 0\right\} \end{aligned} \tag{23}$$

$$\begin{aligned} \beta &= -\Phi^{-1}(P_{\mathrm{f}}) \\ &= -\Phi^{-1} \cdot \\ &\left(1 - P\left\{(F_{\mathrm{s}}-1) \cdot \frac{\dot{W}_1 + \dot{W}_2 - \dot{W}_4}{\int_{\theta_1}^{\theta_2}\int_0^{\sqrt{R^2-l^2}} 2 \cdot w \cdot \left(r_{\mathrm{m}}+l\right)^2 \cdot \cos\theta \big/ \sin\theta \,\mathrm{d}x\mathrm{d}\theta} > 0\right\}\right) \end{aligned} \tag{24}$$

in which R_s is reliability, P_{f} is the failure probability, β is a reliability index, Φ^{-1} is inverse function of standard normal distribution, and $g(X)$ is the function function. X is a vector composed of random variables, that is X=[γ, c, φ, k_h, ζ, σ_{T}].

4. Contrast and validation

Table 1 shows the statistical characteristics of soil parameters and support pressure, and the diameter of tunnel faces D is 10m. Based on the reliability model of the pressurized tunnel faces, Monte Carlo Method (MCM) and response surfaces method (RSM) are used respectively, and the results are shown in Fig. 2 and Table 2. As shown in Fig. 2, with the increase of support pressure σ_{T}, the failure probability P_{f} decreases and the reliability index β increases. When the failure probability is large, the curves calculated by Monte Carlo method and response surface method almost coincide (such as $P_f > 1\times10^{-3}$). When the failure probability decreases gradually, the curve calculated by Monte Carlo method begins to fluctuate, and it can be regarded as taking the response surface method curve as the center line fluctuation.

Suppose that the fluctuation center line is the response

Table 1 Statistical characteristics of random variables

Random variable	Mean value	Standard deviation	Variation coefficient	Distribution type
γ/kN/m^3	18	0.9	5%	Normal
c/kPa	10	2	20%	Normal
φ/°	20	2	10%	Normal
σ_{T}/kPa	-	-	15%	Normal

Table 2 Time-consuming comparison between Monte Carlo method and response surfaces method

Method	MCM (n=2.5×10^5)	MCM (n=1×10^6)	MCM (n=4×10^6)	RSM
Time-consuming /h	2.84	10.86	48.34	0.22

Table 3 Relationship between reliability index and failure probability

Safety level	Reliability index β	Failure probability P_{f}
Safety grade 1	4.2	1.3×10^{-5}
Safety grade 2	3.7	1.1×10^{-4}
Safety grade 3	3.2	6.9×10^{-4}

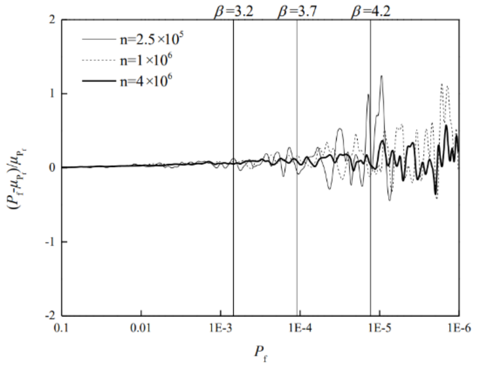

Fig. 3 Curve fluctuation under different sample capacities

surface method curve, when taking different sample capacity, the curve fluctuation calculated by Monte Carlo method is as shown in Fig. 3. In Fig. 3, μ_{Pf} is the failure probability of the centerline, and the ordinate $(P_f-\mu_{Pf})/\mu_{Pf}$ is the ratio of the difference value to the mean value. It can be seen that for the same sample, the smaller the failure probability is, the larger the fluctuation range is; when the failure probability is the same, the larger the sample capacity is, the smaller the curve fluctuation is. It shows that when the sample capacity is fixed, the higher the accuracy of the calculation results, the greater the relative error; under the condition of ensuring accuracy, in order to get more accurate value, the sample capacity need to be increased. According to Fig. 3 and Table 3, the error between the failure probability calculated by n=1×10^6 and n=4×10^6 and the mean value is small ($(P_f-\mu_{Pf})/\mu_{Pf}<1.2$) when the accuracy is ensured (β=4.2 or P_f >1×10^{-4}). Therefore, the sample capacity n=1×10^6 and n=4×10^6 all meet the requirements of 3 safety grades.

It is noteworthy that the failure probability P_f and reliability index β curves of response surfaces method coincide basically with those obtained by Monte Carlo method (n=4×10^6). The feasibility of the response surfaces method and the correctness of the results are verified. In addition, Table 2 shows the calculation time of the two methods (computer parameters: Intel (R) Core (TM) i7-4900 CPU @ 3.60Ghz; 16.0gb RAM; 64 bit). Monte Carlo method (n=4×10^6) takes 48.34h under the calculation accuracy is met, while the response surfaces method only needs 0.22h. To sum up, compared with Monte Carlo method, the response surfaces method is more superior. Therefore, the response surfaces method is used to analyze the reliability of tunnel faces subjected to seismic force.

5. Results analysis

5.1 Influence of soil parameters

5.1.1 Impact of mean

The statistical characteristics of soil parameters and support pressure are shown in Table 4. The diameter of the tunnel faces is D=10 m. The effect of the mean value of cohesion c and internal friction angle φ on failure probability and reliability index of pressurized tunnel faces are shown in Fig. 4 and 5 respectively. With the increase of

Table 4 Statistical characteristics of random variables

Random variable	Mean value	Standard deviation	Variation coefficient	Distribution type
γ/kN/m^3	18	0.9	5%	Normal
c/kPa	6~14	1.2~2.8	20%	Normal
φ/°	10~30	1~3	10%	Normal
σ_T/kPa	-	-	15%	Normal

Table 5 Safety factor and support pressure of pressurized tunnel faces satisfying three safety grades under different shear strength indexes

Shear strength index		Safety factor F_s			Support force σ_T/kPa		
c/kPa	φ/°	Safety grade 3	Safety grade 2	Safety grade 1	Safety grade 3	Safety grade 2	Safety grade 1
6	20	2.4	2.9	3.4	70.7	85.4	100.2
8	20	2.6	3.1	3.7	63.2	75.3	89.9
10	20	3	3.5	4.2	57.4	67.0	80.4
12	20	3.6	4.3	-	50.3	60.1	-
10	10	2.6	3	3.6	141.1	162.8	195.4
10	15	2.8	3.3	3.9	85.9	101.2	119.6
10	20	3	3.5	4.2	57.4	67.0	80.4
10	25	3.2	3.8	4.5	40.8	48.5	57.4
10	30	3.4	4.1	4.9	30.1	36.3	43.4

Table 6 Statistical characteristics of random variables

Random variable	Mean value	Variation coefficient			Distribution type
		Small	General	Large	
γ/kN/m^3	18	3%	5%	8%	Normal
c/kPa	10	15%	20%	25%	Normal
φ/°	20	5%	10%	15%	Normal
σ_T/kPa	-	10%	15%	20%	Normal

the support pressure σ_T, the failure probability P_f is decreasing in the concave curve, and the reliability index β is incremented in the convex curve. With the increase of cohesion c or internal friction angle φ, the failure probability concave curve and the reliability index convex curve become more and more dense. It indicates the curve becomes steeper and the slope becomes larger. However, compared with the cohesion c, the change range of internal friction angle φ is more obvious. Thus, when the support pressure σ_T , cohesion c and internal friction angle φ are large, the collapse probability of pressurized tunnel faces is small and the reliability is greater. Therefore, increasing the support pressure or increasing the shear strength index of soil can effectively reduce the failure probability and increase the reliability of pressurized tunnel faces. In addition, Table 5 shows the safety factor and support pressure required to meet the three safety grades of pressurized tunnel faces under different shear strength indexes.

5.1.2 Influence of variation coefficient

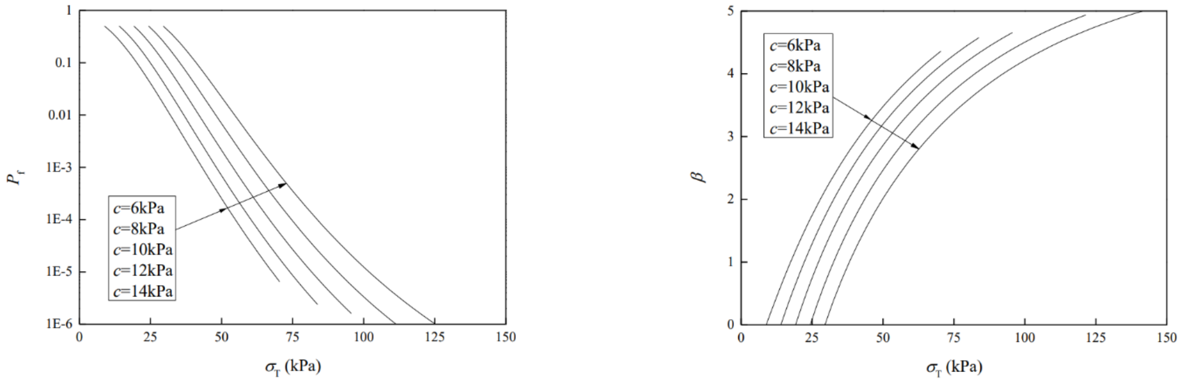

(a) (b)

Fig. 4 Influence of mean value of cohesion on the reliability of pressurized tunnel faces (φ=20°): (a) Failure probability and (b) Reliability index

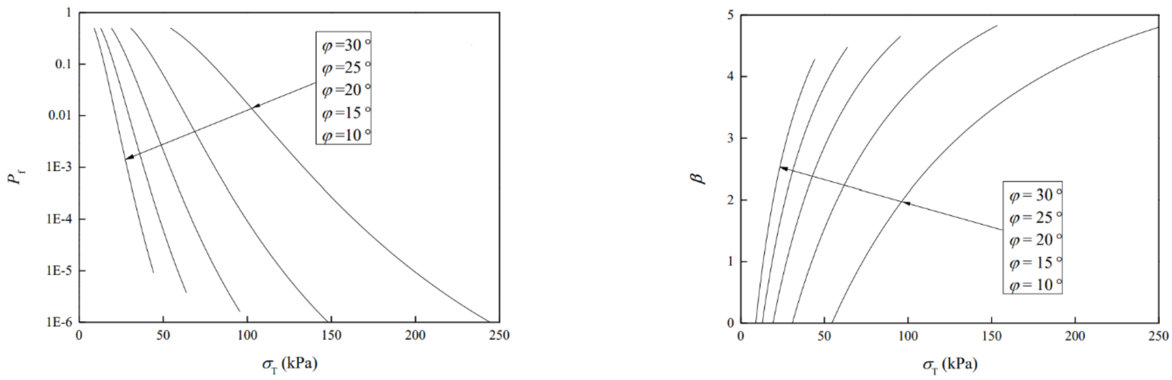

(a) (b)

Fig. 5 Influence of mean value of internal friction angle on the reliability of pressurized tunnel faces (c=10 kPa): (a) Failure probability and (b) Reliability index

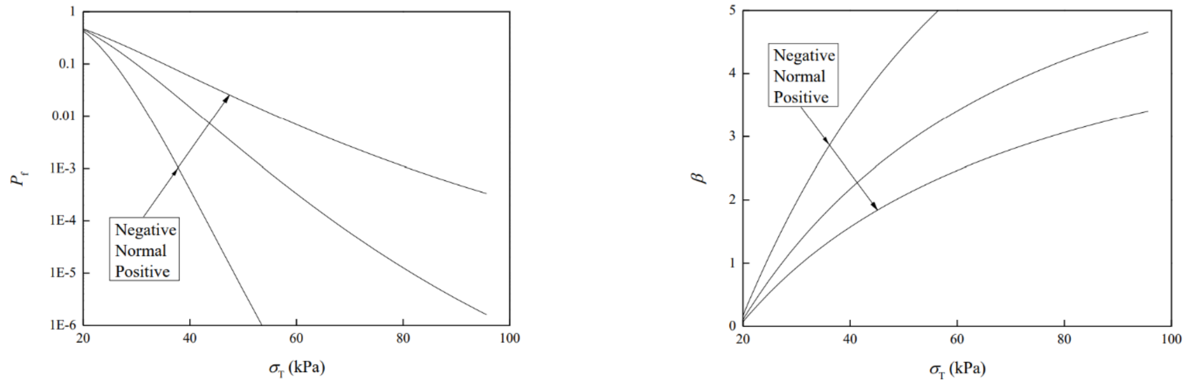

(a) (b)

Fig. 6 Reliability of pressurized tunnel faces under different dispersion degrees: (a) Failure probability and (b) Reliability index

Soil parameters and loads are discrete. The degree of dispersion is generally characterized by the variation coefficient *Cov*. In view of the different dispersion degree of soil parameters and loads, 3 cases with small, general and large variation coefficient are analyzed. The statistical characteristics are as shown in Table 6, and the diameter of tunnel faces is D=10 m. As shown in Fig. 6, when the variation coefficient *Cov* is small, the failure probability of faces P_f is also small, while the reliability index β is larger in the same support pressure σ_T. When the variation coefficient *Cov* is large, the failure probability of faces P_f is larger, the reliability index β is smaller. Thus, the dispersion degree of soil parameters and loads has a significant effect on the reliability of the tunnel faces. The variation coefficient greater, the reliability is worse. Aiming at the small, general and large coefficient variation, the safety factor and support pressure needed to meet the 3 safety grades are given, as shown in Table 7.

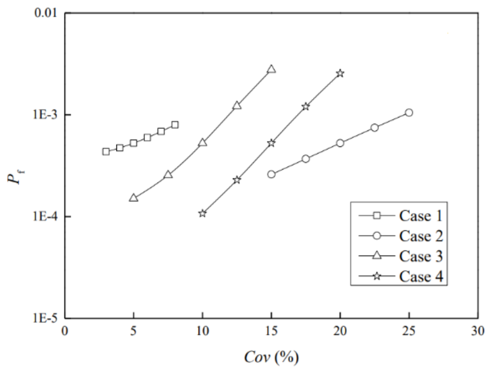

(a)

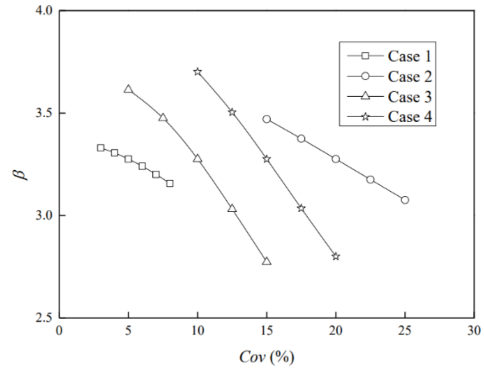

(b)

Fig. 7 Influence of variation coefficients of random variables on the reliability: (a) Failure probability and (b) Reliability index

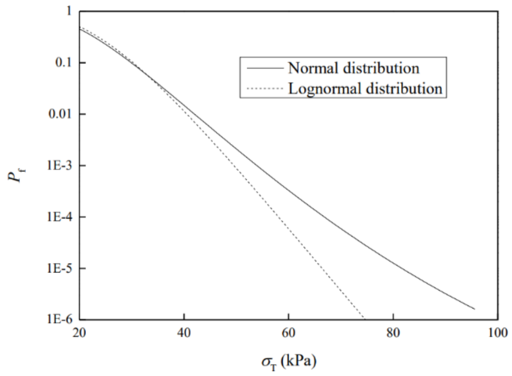

(a)

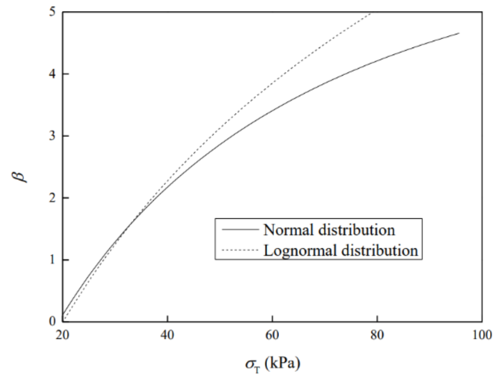

(b)

Fig. 8 Reliability of pressurized tunnel faces under two distribution types: (a) Failure probability and (b) Reliability index

Table 7 Safety factor and support pressure of pressurized tunnel faces satisfying three safety levels under different dispersion degrees

Variation coefficient	Safety grade	Safety factor F_s	Support force σ_T/kPa
Small	3	2.1	40.2
General	3	3	57.4
Large	3	4.5	86.1
Small	2	2.3	44.0
General	2	3.5	67.0
Large	2	>5	-
Small	1	4.2	80.3
General	1	>5	-
Large	1	>5	-

Table 8 Statistical characteristics of random variables

	μ_γ /kN/m^3	μ_c /kPa	μ_φ /°	$\mu_{\sigma T}$ /kPa	Cov_γ /%	Cov_c /%	Cov_φ /%	$Cov_{\sigma T}$ /%	Distribution type
Case 1	18	10	20	57.4	3~8	20	10	15	Normal
Case 2	18	10	20	57.4	5	15~25	10	15	Normal
Case 3	18	10	20	57.4	5	20	5~15	15	Normal
Case 4	18	10	20	57.4	5	20	10	10~20	Normal

Table 9 Statistical characteristics of random variables

Random variable	Mean value	Standard deviation	Variation coefficient	Distribution type
γ/kN/m^3	18	0.9	5%	Normal or lognormal
c/kPa	10	2	20%	Normal or lognormal
φ/°	20	2	10%	Normal or lognormal
σ_T/kPa	-	-	15%	Normal or lognormal

Table 10 Safety factor and support pressure of pressurized tunnel faces satisfying three safety grades under two distribution types

Safety grade	Safety factor F_s		Support force σ_T/kPa		Relative error Δ/%
	Normal distribution	Lognormal distribution	Normal distribution	Lognormal distribution	
3	3.0	2.7	57.4	51.7	10
2	3.5	3.1	67.0	59.3	11
1	4.2	3.5	80.3	67.0	17

Note: Relative error Δ=|σ_T(normal distribution)-σ_T(lognormal distribution)|/σ_T(normal distribution)

To analyze the impact of variation coefficient of each random variable on the reliability of the pressurized tunnel faces, the statistical characteristics of four sets of random variables are assumed, which is shown in Table 8. As shown in Fig. 7, the failure probability P_f of pressurized tunnel faces increases and the reliability index β decreases in different degrees with the increase of the variation

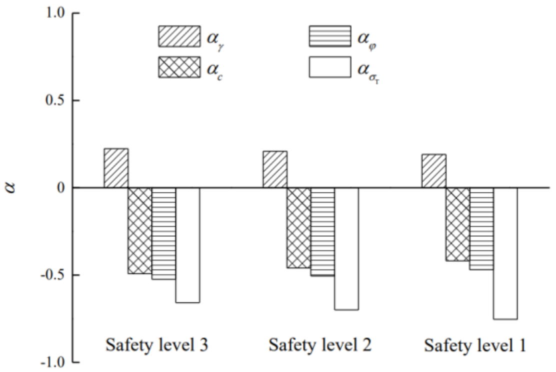

Fig. 9 Comparison of sensitivity coefficient under three safety grades

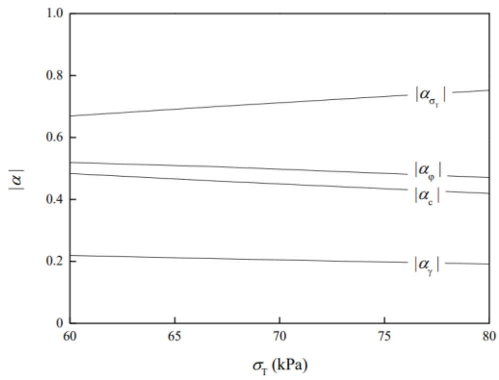

Fig. 10 Variation rule of absolute value of sensitivity coefficients with support pressure

Table 11 Statistical characteristics of random variables

Random variable	Mean value	Standard deviation	Variation coefficient	Distribution type
γ/kN/m^3	18	0.9	5%	Normal
c/kPa	10	2	20%	Normal
φ/°	20	2	10%	Normal
σ_T/kPa	-	-	15%	Normal

Table 12 Sensitivity coefficient of random variables

	σ_T/kPa	α_γ	α_c	α_φ	$\alpha_{\sigma T}$
Safety grade 3	57.4	0.22	-0.49	-0.52	-0.66
Safety grade 2	67.0	0.21	-0.46	-0.51	-0.70
Safety grade 1	80.4	0.19	-0.42	-0.47	-0.75

coefficient *Cov* in the corresponding range of variation. Compared with cohesion c and soil weight γ, the effect of internal friction angle φ and support pressure σ_T is more significant. It shows that the dispersion degree of internal friction angle φ and support pressure σ_T have great influence on the reliability. The influence of the cohesion c and the soil weight σ_T is relatively small.

5.1.3 Impact of distribution types

Soil parameters and loads are generally subject to normal distribution or logarithmic normal distribution (Mollon *et al*. 2013). Assuming that the statistical characteristics of a random variable are shown in Table 9, the diameter of tunnel faces is D=10 m. The reliability of pressurized tunnel faces based on two distribution types is shown in Fig. 8. When the support pressure $\sigma_T \leq 40$ kPa, the two curves basically coincide. While the two curves gradually separate and the error is getting bigger and bigger with the increase of the support pressure σ_T. Generally, the reliability based on normal distribution is small. The reliability based on the logarithmic normal distribution is large. As can be found from Table 10, the relative errors of the results based on the two distribution types are 10%, 11%, 17% respectively under satisfying three safety grades. Thus, the distribution types of soil parameters and loads also have a great influence on the reliability of pressurized tunnel faces.

Table 13 Statistical characteristics of random variables

Random variable	Mean value	Standard deviation	Variation coefficient	Distribution type
γ/kN/m^3	18	0.9	5%	Normal
c/kPa	10	2	20%	Normal
φ/°	20	2	10%	Normal
σ_T/kPa	-	-	15%	Normal

5.1.4 Sensitivity

Sensitivity characterizes the influence of random variables on reliability indexes. The importance of random variables to structural stability can be obtained by sensitivity analysis. The sensitivity coefficient of random variable X_i is α_{X_i} .

Table 11 shows the statistical characteristics of random variables. The sensitivity coefficients of each random variable are shown in Table 12. For ease of analysis, the data of Table 12 is plotted in Fig. 9 and 10. As can be found in Fig. 9, the sensitivity coefficient α_{σ_T} , α_φ and α_c are negative, which has a positive effect on the reliability of pressurized tunnel faces. α_γ is positive, it has a negative effect on the reliability of pressurized tunnel faces. As can be determined by Fig. 10, according to the absolute value of the sensitivity coefficient, the influence degree of random variables on the reliability is as follows: The support pressure σ_T is the largest, followed by the internal friction angle φ, then the cohesion c , the soil weight γ is the smallest. With the increase of support pressure σ_T, the absolute value of sensitivity coefficient $|\alpha_{\sigma_T}|$ increases, $|\alpha_\varphi|$, $|\alpha_c|$ and $|\alpha_\gamma|$ decrease. It indicates that the influence of support pressure σ_T on reliability is increasing. The influence of internal friction angle φ, cohesion c and soil weight γ on the reliability of pressurized tunnel faces is decreasing. The increase effect of support pressure σ_T is more obvious, the reduction effect of cohesion c and internal friction angle φ is weaker, the soil weight degree γ is more stable, and the reduction effect is not obvious.

5.1.5 Correlation impact of c and φ

In the previous reliability analysis, it was assumed that the random variables were independent of each other. However, there may be some correlation between the soil

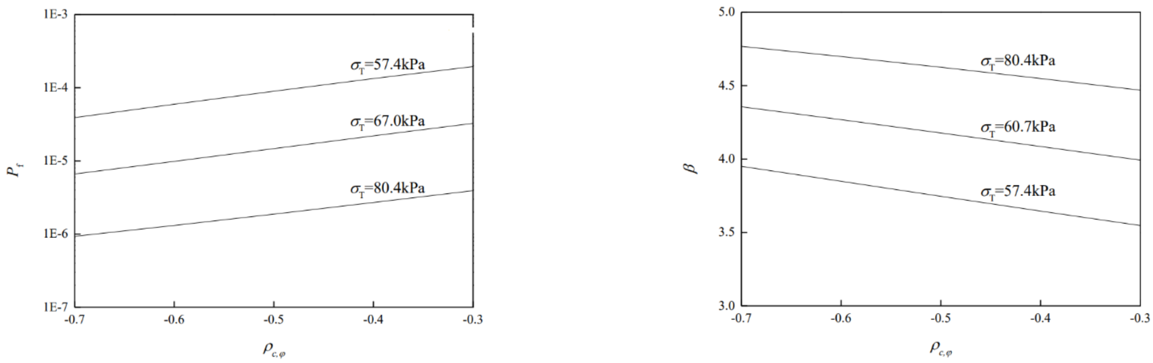

(a) (b)

Fig. 11 Influence of correlation coefficient $\rho_{c,\varphi}$ on the reliability of pressurized tunnel faces: (a) Failure probability and (b) Reliability index

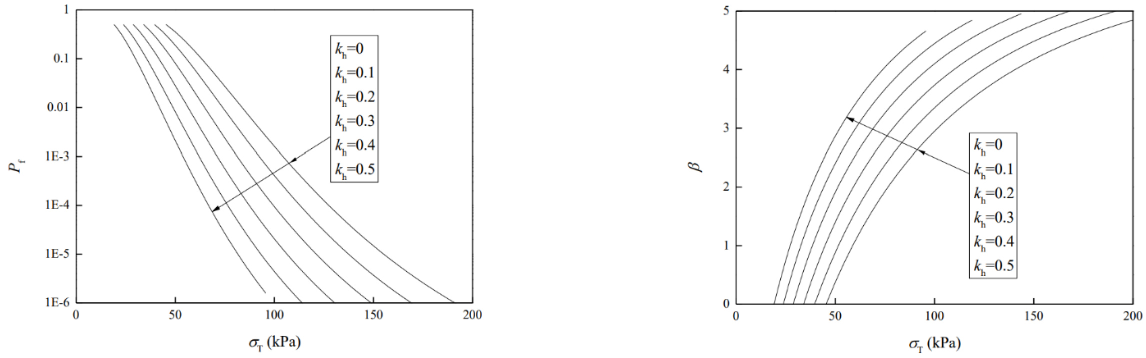

(a) (b)

Fig. 12 The influence of k_h on the reliability of pressurized tunnel faces: (a) Failure probability and (b) Reliability index

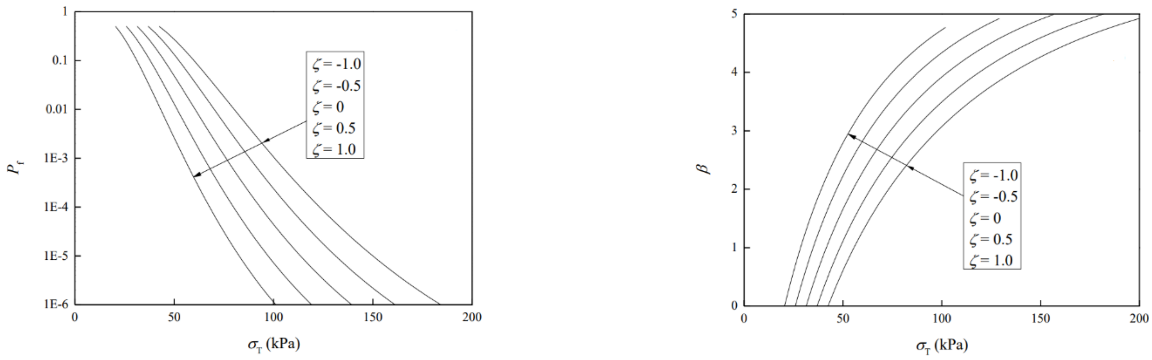

(a) (b)

Fig. 13 The influence of ζ on the reliability of pressurized tunnel faces: (a) Failure probability and (b) Reliability index

Table 14 Reliability comparison of pressurized tunnel faces under different correlation coefficients $\rho_{c,\varphi}$

$\rho_{c,\varphi}$	σ_T=57.4kPa			σ_T=67.0kPa			σ_T=80.4kPa		
	P_f	β	Δ/%	P_f	β	Δ/%	P_f	β	Δ/%
-0.7	3.9×10^{-5}	3.95	20.8	6.6×10^{-6}	4.36	17.2	9.3×10^{-7}	4.77	13.0
-0.6	5.9×10^{-5}	3.85	17.7	9.8×10^{-6}	4.27	14.8	1.3×10^{-6}	4.70	11.4
-0.5	9.0×10^{-5}	3.75	14.7	1.5×10^{-5}	4.18	12.4	1.9×10^{-6}	4.63	9.7
-0.4	1.3×10^{-4}	3.65	11.6	2.2×10^{-5}	4.09	9.9	2.7×10^{-6}	4.55	7.8
-0.3	2.0×10^{-4}	3.55	8.6	3.3×10^{-5}	3.99	7.3	3.9×10^{-6}	4.47	5.9
0	5.3×10^{-4}	3.27	-	9.8×10^{-5}	3.72	-	1.2×10^{-5}	4.22	-

Note: Relative error $\Delta=\left|\beta_{\rho\neq0}-\beta_{\rho=0}\right|/\beta_{\rho=0}$

Table 15 Statistical characteristics of random variables

Random variable	Mean value	Standard deviation	Variation coefficient	Distribution type
γ/kN/m^3	18	0.9	5%	Normal
c/kPa	10	2	20%	Normal
φ/°	20	2	10%	Normal
k_h	0~0.5	0~0.75	15%	Normal
σ_T/kPa	-	-	15%	Normal

parameters. The soil shear strength indexes, cohesion and internal friction angle, are taken as examples, the influence of the correlation between them on the reliability of

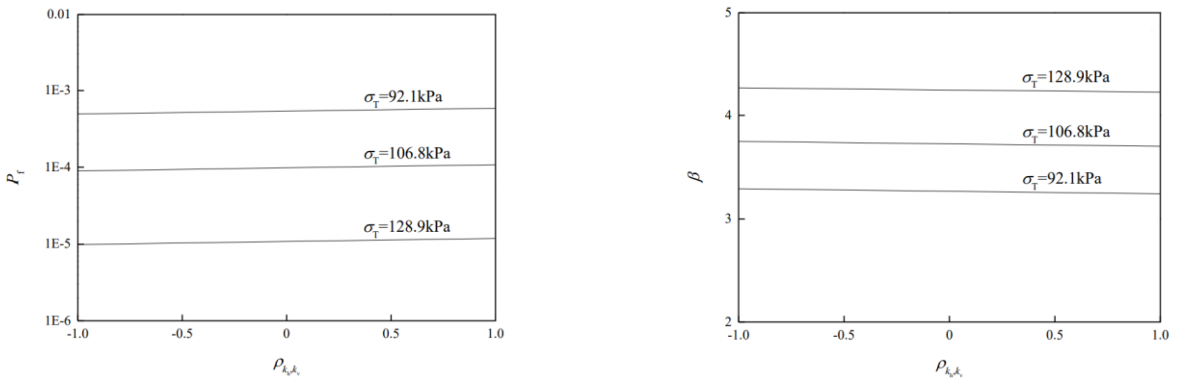

(a) (b)

Fig. 14 The influence of correlation coefficient ρ_{k_h,k_v} on the reliability of pressurized tunnel faces: (a) Failure probability; (b) Reliability index

Table 16 Statistical characteristics of random variables

Random variable	Mean value	Standard deviation	Variation coefficient	Distribution type
γ/kN/m^3	18	0.9	5%	Normal
c/kPa	10	2	20%	Normal
φ/°	20	2	10%	Normal
k_h	0.25	0.0375	15%	Normal
ζ	-1~1	0~0.15	15%	Normal
σ_T/kPa	-	-	15%	Normal

Table 17 Statistical characteristics of random variables

Random variable	Mean value	Standard deviation	Variation coefficient	Distribution type
γ/kN/m^3	18	0.9	5%	Normal
c/kPa	10	2	20%	Normal
φ/°	20	2	10%	Normal
k_h	0.25	0.0375	15%	Normal
k_v	0.125	0.01875	15%	Normal
σ_T/kPa	-	-	15%	Normal

Table 18 Reliability comparison of pressurized tunnel faces under different correlation coefficients ρ_{k_h,k_v}

ρ_{k_h,k_v}	σ_T=92.1kPa			σ_T=106.8kPa			σ_T=128.9kPa		
	P_f	β	Δ/%	P_f	β	Δ/%	P_f	β	Δ/%
-1.0	4.9×10^{-4}	3.29	0.6	8.9×10^{-5}	3.75	0.8	9.9×10^{-6}	4.27	0.5
-0.5	5.2×10^{-4}	3.28	0.3	9.4×10^{-5}	3.74	0.5	1.0×10^{-5}	4.26	0.2
0	5.4×10^{-4}	3.27	-	9.8×10^{-5}	3.72	-	1.1×10^{-5}	4.25	-
0.5	5.6×10^{-4}	3.26	0.3	1.0×10^{-4}	3.71	0.3	1.1×10^{-5}	4.24	0.2
1.0	5.9×10^{-4}	3.24	0.9	1.1×10^{-4}	3.70	0.5	1.2×10^{-5}	4.23	0.5

Note: Relative error $\Delta=\left|\beta_{\rho\neq0}-\beta_{\rho=0}\right|/\beta_{\rho=0}$

pressurized tunnel faces is analyzed. According to the existing research results (Lü *et al*. 2011), there is a negative correlation between c and φ. The range of correlation coefficient $\rho_{c,\varphi}$ is generally -0.7~-0.3.

Assuming that the statistical characteristics of random variables are shown in Table 13, the results are presented in Fig. 11 and Table 14. It can be known from Fig. 11 and Table 14, the greater the negative correlation between c and φ, the smaller the failure probability of the tunnel faces, the greater the reliability index. Ignoring the negative correlation between them, the failure probability will become larger, the reliability index will become smaller. When the requirements of three different safety grades are met, that is, β= 3.2, 3.5, 4.2, the maximum relative error of failure probability is 20.8%, 17.2% and 13%, respectively.

5.2 Effects of seismic force

5.2.1 Influence of horizontal seismic force

Table 15 shows the statistical characteristics of random variables only considering horizontal seismic loads. The results are shown in Fig. 12. With the support pressure σ_T increases, the failure probability P_f is decreasing by a concave curve, and the reliability index β is incremented by convex curve. With the increase of horizontal seismic acceleration coefficient k_h, the failure probability P_f increases while the reliability index β decreases. If the influence of horizontal seismic load is ignored, that is, k_h =0, the reliability index of pressurized tunnel faces will be overestimated.

5.2.2 Influence of vertical seismic force

Table 16 is the statistical characteristics of random variables considering the simultaneous action of horizontal seismic loads and vertical seismic loads. The results are shown in Fig. 13. With the increase of ratio coefficient ζ of vertical seismic acceleration, the failure probability P_f increases, the reliability index β decreases. If the influence of vertical seismic load is ignored, that is, ζ=0, the results will produce a large error.

5.2.3 Influence of the correlation of k_h and k_v

The statistical characteristics of random variables are shown in Table 17. Considering the correlation between horizontal seismic loads and vertical seismic loads, the results are shown in Fig. 14 and Table 18. From Table 18, under the action of 3 kinds of support pressure 92.1kPa, 106.8kPa and 128.9kPa, if the correlation between horizontal and vertical seismic load is not taken into account, that is, $\rho_{k_h,k_v}=0$, the reliability of pressurized tunnel faces is satisfied with 3 safety grades respectively. If the correlation is considered, that is, $\rho_{k_h,k_v}\neq 0$, as the correlation coefficient ρ_{k_h,k_v} increases, the failure probability P_f linearly increases, the reliability index β linearly decreases, but the effect is not obvious (shown in Fig. 14). Compared with $\rho_{k_h,k_v}=0$, the maximum relative errors of reliability indexes are 0.9%, 0.8% and 0.5%, respectively. Thus, the correlation between horizontal and vertical seismic load has little effect on the reliability index of pressurized tunnel faces. The negative correlation slightly improves the reliability index; the positive correlation slightly reduces the reliability index. It can be assumed that the horizontal seismic load and the vertical seismic load are independent of each other and ignoring the influence of its correlation under the condition that the accuracy requirement is not high.

6. Conclusions

• The reliability of pressurized tunnel faces was solved by the response surfaces method (RSM) and Monte Carlo method (MCM) respectively. The results of MCM are closely related to the sample capacity n. When the sample capacity is $n=1\times10^6$, the results obtained based on MCM are basically consistent with these obtained by RSM. The feasibility of the response surfaces method is verified. When the accuracy is satisfied, the RSM only takes 0.086 hour, while MCM ($n=1\times10^6$) takes 9.70 hours. So the RSM is more superior.

• The statistical characteristics, such as support pressure and soil parameters, variation coefficients and the distribution type, have great influence on the reliability of pressurized tunnel faces. Sensitivity analysis shows that the random variables affecting the reliability of faces are in turn: support pressure σ_T, internal friction angle φ, cohesion c, and soil weight γ. In addition, there is a negative correlation between soil cohesion c and internal friction angle φ. And the relationship significantly affects the reliability of pressurized tunnel faces. The reliability will be underestimated if ignored the negative correlation, and the maximum relative error of reliability are 20.8%, 17.2% and 13% under 3 safety grades.

• The reliability of faces decreases significantly when the horizontal or vertical seismic force increases. While the correlation between horizontal and vertical seismic forces has little effect on the reliability of tunnel faces, and the correlation between them can be ignored when the accuracy is not high.

Acknowledgments

All authors thank the financial support by the National Natural Science Foundation of China (51804113, 51674115 and 51974118), Scientific Research Fund of Hunan Provincial Education Department (17B095) and Natural Science Foundation of Hunan Province (2019JJ40082) for this research work.

References

Anagnostou, G. and Perazzelli, P. (2013), "The stability of a tunnel face with a free span and a non-uniform support", *Geotechnik*, **36**(1), 40-50. https://doi.org/10.1002/gete.201200014.

Clot, A., Romeu, J. and Arcos, R. (2016), "An energy flow study of a double-deck tunnel under quasi-static and harmonic excitations", *Soil Dyn. Earthq. Eng.*, **89**, 1-4. https://doi.org/10.1016/j.soildyn.2016.07.008.

Hernández, Y.Z., Farfán, A.D. and de Assis, A.P. (2019), "Three-dimensional analysis of excavation face stability of shallow tunnels", *Tunn. Undergr. Sp. Technol.*, **92**, 103062. https://doi.org/10.1016/j.tust.2019.103062.

Huang, F., Zhang, M., Wang, F., Ling, T.H. and Yang, X.L. (2020), "The failure mechanism of surrounding rock around an existing shield tunnel induced by an adjacent excavation", *Comput. Geotech.*, **117**, 103236. https://doi.org/10.1016/j.compgeo.2019.103236.

Huang, F., Zhao, L.H., Ling, T.H. and Yang, X.L. (2017), "Rock mass collapse mechanism of concealed karst cave beneath deep tunnel", *Int. J. Rock Mech. Min. Sci.*, **91**, 133-138. https://doi.org/10.1016/j.ijrmms.2016.11.017.

Ibrahim, E., Soubra, A.H., Mollon, G., Raphael, W., Dias, D. and Reda, A. (2015), "Three-dimensional face stability analysis of pressurized tunnels driven in a multilayered purely frictional medium", *Tunn. Undergr. Sp. Technol.*, **49**(1), 18-34. https://doi.org/10.1016/j.tust.2015.04.001.

Kim, S.H. and Tonon, F. (2010), "Face stability and required support pressure for TBM driven tunnels with ideal face membrane-Drained case", *Tunn. Undergr. Sp. Technol.*, **25**(5), 526-542. https://doi.org/10.1016/j.tust.2010.03.002.

Leca, E. and Dormieux, L. (1990), "Upper and lower bound solutions for the face stability of shallow circular tunnels in frictional material", *Geotechnique*, **40**(4), 581-606. https://doi.org/10.1680/geot.1990.40.4.581.

Liang, Q., Yang, X.L., Zhang, J.H. and Zhou, W.Q. (2016), "Upper bound analysis for supporting pressure of shield tunnel in heterogeneous soil", *Rock Soil Mech.*, **37**(9), 2585-2592. (in Chinese). https://doi.org/10.16285/j.rsm.2016.09.020.

Lü, Q., Sun, H.Y. and Low, B.K. (2011), "Reliability analysis of ground-support interaction in circular tunnels using the response surface method", *Int. J. Rock Mech. Min. Sci.*, **48**(8), 1329-1343. https://doi.org/10.1016/j.ijrmms.2011.09.020.

Mollon, G., Dias, D. and Soubra, A.H. (2011), "Rotational failure mechanisms for the face stability analysis of tunnels driven by a pressurized shield", *Int. J. Numer. Anal. Meth. Geomech.*, **35**(12), 1363-1388. https://doi.org/10.1002/nag.962.

Mollon, G., Dias, D. and Soubra, A.H. (2013), "Range of the safe retaining pressures of a pressurized tunnel face by a probabilistic approach", *J. Geotech. Geoenviron. Eng.*, **139**(11), 1954-1967. https://doi.org/10.1061/(ASCE)GT.1943-5606.0000911.

Pan, Q.J. and Dias, D. (2018), "Three dimensional face stability of a tunnel in weak rock masses subjected to seepage forces", *Tunn. Undergr. Sp. Technol.*, **71**, 555-566. https://doi.org/10.1016/j.tust.2017.11.003.

Saada, Z., Maghous, S. and Garnier, D. (2013), "Pseudo-static analysis of tunnel face stability using the generalized Hoek-Brown strength criterion", *Int. J. Numer. Anal. Meth. Geomech.*, **37**(18), 3194-3212. https://doi.org/10.1002/nag.2185.

Sahoo, J.P. and Kumar, B. (2019), "Support pressure for stability of circular tunnels driven in granular soil under water table", *Comput. Geotech.*, **109**, 58-68. https://doi.org/10.1016/j.compgeo.2019.01.005.

Senent, S., Mollon, G. and Jimenez, R. (2013), "Tunnel face stability in heavily fractured rock masses that follow the Hoek-Brown failure criterion", *Int. J. Rock Mech. Min. Sci.*, **60**(1), 440-451. https://doi.org/10.1016/j.ijrmms.2013.01.004.

Subrin, D. and Wong, H. (2002), "Tunnel face stability in frictional material: a new 3D failure mechanism", *CR Mecanique*, **330**(7), 513-519. https://doi.org/10.1016/S1631-0721(02)01491-2.

Su, Y.H., Zhang, P. and Zhao, M.H. (2007), "Improved response surface method and its application in stability reliability degree analysis of tunnel surrounding rock", *J. Central South Univ. Sci. Technol.*, **14**(6), 870-876. https://doi.org/10.1007/s11771-007-0165-2.

Shrestha, P.K. and Panthi, K.K. (2014), "Groundwater effect on faulted rock mass: an evaluation of Modi Khola pressure tunnel in the Nepal Himalaya", *Rock Mech. Rock Eng.*, **47**(3), 1021-1035. https://doi.org/10.1007/s00603-013-0467-7.

Wu, Q.H., Weng, L., Zhao, Y.L., Guo, B.H, and Luo, T. (2019), "On the tensile mechanical characteristics of fine-grained granite after heating/cooling treatments with different cooling rates", *Eng. Geol.*, **253**, 94-110. https://doi.org/10.1016/j.enggeo.2019.03.014.

Yang, Z.H., Yang, X.L., Zhang, J.H., and Li, Y.X. (2015), "Upper bound analysis of collapsing area of tunnel face in broken soft rocks under different saturations", *J. Central South Univ. Technol.*, **46**(6), 2267-2273 (in Chinese). https://doi.org/10.11817/j.issn.1672-7207.2015.06.

Zhang, B., Wang, X., Zhang, J.S. and Meng, F. (2017), "Three-dimensional limit analysis of seismic stability of tunnel faces with quasi-static method", *Geomech. Eng.*, **13**(2), 301-318. https://doi.org/10.12989/gae.2017.13.2.301.

Zhang, D.B., Jiang, Y. and Yang, X.L. (2019b), "Estimation of 3D active earth pressure under nonlinear strength condition", *Geomech. Eng.*, **17**(6), 515-525. https://doi.org/10.12989/gae.2019.17.6.515.

Zhang, J.H., Wang, W.J., Zhang, B. and Zhang, D.B. (2019a), "Upper bound analysis for collapse failure of shield tunnel face excavated in unsaturated soils considering steady vertical flow", *Math Probl. Eng.*, Article ID 2145616. https://doi.org/10.1155/2019/2145616.

Zhang, J.H., Wang, W.J., Zhang, D.B., Zhang, B. and Meng, F. (2018), "Safe range of retaining pressure for three-dimensional face of pressurized tunnels based on limit analysis and reliability method", *KSCE J. Civ. Eng.*, **22**(11), 4645-4656. https://doi.org/10.1007/s12205-017-0619-5.

Zhang, Z.Z., Deng, M., Bai, J.B., Yu, X.Y., Wu, Q.H. and Jiang, L.S. (2020), "Strain energy evolution and conversion under triaxial unloading confining pressure tests due to gob-side entry retained", *Int. J. Rock Mech. Min. Sci.*, **126**, 104184. https://doi.org/10.1016/j.ijrmms.2019.104184.

Zhang, Z.Z., Yu, X.Y., Wu, H. and Deng, M. (2019c), "Stability control for gob-side entry retaining with supercritical etained entry width in thick coal seam longwall mining", *Energies*, **12**(7), 1375. https://doi.org/10.3390/en12071375.

CC